EDGE ARTICLE

CrossMark
click for updates

The approach to 4d/4f-polyphosphides†

Nicholas Arleth,[a] Michael T. Gamer,[a] Ralf Köppe,[a] Nikolay A. Pushkarevsky,[bc]
Sergey N. Konchenko,[ab] Martin Fleischmann,[c] Michael Bodensteiner,[c]
Manfred Scheer[c] and Peter W. Roesky*[a]

The first 4d/4f polyphosphides were obtained by reaction of the divalent metallocenes [Cp*$_2$Ln(thf)$_2$] (Ln = Sm, Yb) with [{CpMo(CO)$_2$}$_2$(μ,$\eta^{2:2}$-P$_2$)] or [Cp*Mo(CO)$_2$(η^3-P$_3$)]. Treatment of [Cp*$_2$Ln(thf)$_2$] (Ln = Sm, Yb) with [{CpMo(CO)$_2$}$_2$(μ,$\eta^{2:2}$-P$_2$)] gave the 16-membered bicyclic compounds [(Cp$_2$*Ln)$_2$P$_2$(CpMo(CO)$_2$)$_4$] (Ln = Sm, Yb) as the major products. From the reaction involving samarocene, the cyclic P$_4$ complex [(Cp*$_2$Sm)$_2$P$_4$(CpMo(CO)$_2$)$_2$] and the cyclic P$_5$ complex [(Cp*$_2$Sm)$_3$P$_5$(CpMo(CO)$_2$)$_3$] were also obtained as minor products. In each reaction, the P$_2$ unit is reduced and a rearrangement occurred. In dedicated cases, a P–P bond formation takes place, which results in a new aggregation of the central phosphorus scaffold. In the reactions of [Cp*$_2$Ln(thf)$_2$] (Ln = Sm, Yb) with [Cp*Mo(CO)$_2$P$_3$] a new P–P bond is formed by reductive dimerization and the 4d/4f hexaphosphides [(Cp*$_2$Ln)$_2$P$_6$(Cp*Mo(CO)$_2$)$_2$] (Ln = Sm, Yb) were obtained.
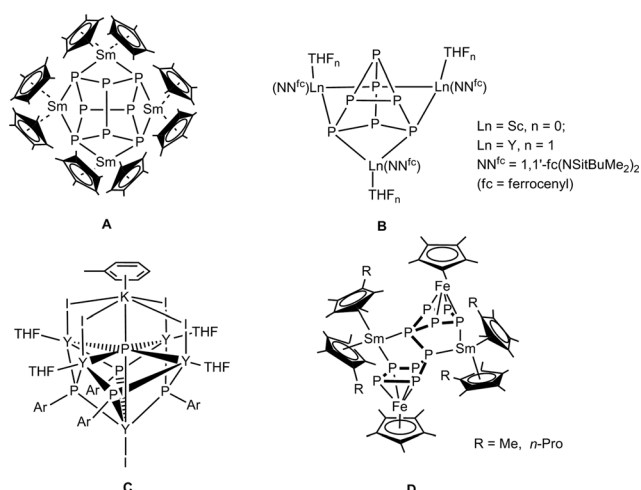
Introduction

Phosphorus is one of the most common and well-established donor atoms in coordination chemistry, and it can form strong bonds with soft metals.[1–3] Many transition metal phosphorus complexes are used as catalysts in various industrial processes.[4] In contrast, rare-earth metal phosphorus complexes are far less common[5] and only a few years ago the first molecular lanthanide polyphosphide complex, [(Cp*$_2$Sm)$_4$P$_8$] (Cp* = η^5-C$_5$Me$_5$) (**A**, Scheme 1),[6] was reported. It was obtained by reaction of the divalent solvate-free samarocene [Cp*$_2$Sm] with white phosphorus. The structure can be described as a realgar-shaped P$_8^{4-}$ ligand trapped in a cage of four samarocenes. Another example of direct activation of P$_4$ to a ligand-stabilized P$_8^{4-}$ was reported by Diaconescu and coworkers. [{(NN^{fc})Sc}$_4$P$_8$] (NN^{fc} = 1,1′-fc(NSitBuMe$_2$)$_2$, fc = ferrocenylene) was obtained by the reaction of P$_4$ and 1 equiv. of the scandium naphthalene complex [{(NN^{fc})Sc}$_2$(μ-C$_{10}$H$_8$)].[7] Using this methodology, the P$_7^{3-}$ compounds [{(NN^{fc})Ln(THF)$_n$}$_3$P$_7$] (Ln = Sc, Y, La, Lu; **B**, Scheme 1) were also reported.[7,8] The first well-defined P^{3-}-containing rare-earth metal compounds, in which six yttrium atoms coordinate to a μ_6-P^{3-} ligand, were synthesized by Chen and coworkers (**C**, Scheme 1).[9] Recently, we reported the reactions of divalent samarium compounds with transition-metal-

coordinated polyphosphides.[10,11] In this context, the first P–P bond formation reactions between two [Cp*FeP$_5$] molecules triggered by divalent lanthanide complexes to give [(Cp*Fe)$_2$-P$_{10}${Sm(η^5-C$_5$Me$_4$R)$_2$}$_2$] (R = Me, nPr; **D**, Scheme 1) were reported. This intermolecular P–P bond formation arises from reductive dimerization.[12,13]

Since the existing examples of lanthanide/polyphosphide complexes came from 3d transition metal complexes, the question arises, whether 4d metals will follow this reactivity mode or novel transformations will occur. Herein, we report the first 4d/4f polyphosphides containing unprecedented polyphosphorus moieties, which were formed by multiple intermolecular P–P bond formations and untypical metal fragment motions.

^{a}Institute of Inorganic Chemistry, Karlsruhe Institute of Technology, Engesserstrasse 15, 76131 Karlsruhe, Germany. E-mail: roesky@kit.edu

^{b}Nikolaev Institute of Inorganic Chemistry SB RAS, Novosibirsk State University, Prosp. Lavrentieva 3, Pirogova str. 2, 630090 Novosibirsk, Russia. E-mail: konch@niic.nsc.ru

^{c}Institute of Inorganic Chemistry, University of Regensburg, 93040 Regensburg, Germany. E-mail: Manfred.Scheer@chemie.uni-regensburg.de

† Electronic supplementary information (ESI) available. CCDC 1402049-1402054. For ESI and crystallographic data in CIF or other electronic format see DOI: 10.1039/c5sc02252e

Scheme 1 Known lanthanide polyphosphide complexes.[6–9,13]

Results and discussion

Reactions of $[Cp*_2Ln(thf)_2]$ (Ln = Sm, Yb),[14–16] with $[\{CpMo(CO)_2\}_2(\mu,\eta^{2:2}-P_2)]$[17] at 60 °C in toluene for one week yielded a product mixture, which could be separated by fractional crystallization. The 16-membered bicyclic compounds $[(Cp*_2Ln)_2P_2(CpMo(CO)_2)_4]$ (Ln = Sm (**1a**), Yb (**1b**)) were the major products (Scheme 2). From the reaction with samarocene, the cyclic P_4 complex $[(Cp*_2Sm)_2P_4(CpMo(CO)_2)_2]$ (**2**) and the cyclic P_5 complex $[(Cp*_2Sm)_3P_5(CpMo(CO)_2)_3]$ (**3**) were obtained as minor products (Scheme 2).

Fractional crystallization of the mother liquor afforded **1a** first, allowing for it to be fully characterized. Further concentration resulted in a mixture of **1a**, **2** and **3**, and some poorly soluble powder, which could not be further identified. The crystals of **2** and **3** could only be separated manually and, thus, a complete characterization was not possible. Nevertheless, the solid-state structures give insight into the reaction pathway.

In all cases, the lanthanide atoms in $[Cp*_2Ln(thf)_2]$ are oxidized from oxidation state +2 to +3.[18] The oxidation state of the samarium atom was clearly assigned by NIR spectroscopy (see below) and magnetic measurements. Concomitant with the oxidation of the lanthanide atom, the polyphosphide is reduced. Furthermore, upon reduction, in **2** and **3** the Mo–Mo bond is completely broken and $\{CpMo(CO)_2\}$ fragments without any metal-to-metal bond are formed. Each of these $\{CpMo(CO)_2\}$ units also coordinates to a polyphosphide for electronic saturation, resulting in 18 VE species.

Compounds **1a,b** are crystallographically similar but due to different amounts of lattice solvent not isostructural. They both crystallize in the triclinic space group $P\bar{1}$ (Fig. 1). In **1a,b** two phosphorus atoms form a central $\{P=P\}^{2-}$ unit, which coordinates end-on to two $\{CpMo(CO)_2\}_2$ fragments. There is only one other example known of such a P_2 unit four times coordinated by $Cp*Re(CO)_2$ moieties.[19] A crystallographic inversion center is observed in the center of the $\{P=P\}^{2-}$ unit. The P–P bond distances of 2.029(4) Å (**1a**) and 2.007(4) Å (**1b**) are in the range of a P=P double bond (e.g. 2.052(2) Å in $[(Cp'''Co)_2(\mu,\eta^{2:2}-P_2)_2]$ ($Cp''' = 1,2,4\text{-}tBu_3C_5H_2$)[20] and are slightly shorter than in the starting material $[\{CpMo(CO)_2\}_2(\mu,\eta^{2:2}-P_2)]$ (P–P 2.079(2) Å).[17] The Mo–P distances in **1a** (av. 2.366 Å) and **1b** (av. 2.360 Å) are significantly shorter than in $[\{CpMo(CO)_2\}_2(\mu,\eta^{2:2}-P_2)]$ (2.552(1) Å and 2.463(1) Å). The Mo–Mo bonds of 3.1935(8) Å (**1a**) and 3.2073(9) Å (**1b**) are in the upper range of unsupported Mo–Mo bonds (2.88–3.32 Å).[21]

The central $\{P_2(CpMo(CO)_2)_4\}^{2-}$ subunit is end-capped by two $\{Cp*_2Ln\}^+$ units, each coordinating via two isocarbonyl bridges to the central core. Thus, a 16-membered bicyclic structure is formed, which consists of the $\{P=P\}^{2-}$ unit, four Mo atoms, two Ln atoms, and four carbonyl ligands each bridging the Ln and Mo atoms. The Ln–O bond distances of the isocarbonyl bridges (Sm–O2 2.359(5) Å and Sm–O4 2.389(5) Å; Yb–O2 2.231(5) Å and Yb–O4 2.246(5) Å) are in the range of other isocarbonyl compounds, e.g. $[(Tp^{Me,Me})_2Sm(\mu\text{-}CO)\{Cp^{Me}Mo(CO)_2\}]$ (2.335(4) Å; $Tp^{Me,Me}$ = (2,4-dimethyl-pyrazolyl)$_3$borate, Cp^{Me} = MeC_5H_4);[22] and $[(SmI_2(thf)_4)(\mu\text{-}CO)(CpMo(CO)_2)]$ (2.41(2) Å and 2.49(2) Å).[20] The lanthanide atoms are coordinated to two isocarbonyl ligands and two Cp* rings, resulting in a distorted tetrahedral coordination geometry. As a result of the oxidation of the lanthanide atoms, the average Ln–C bond is shortened by about 0.2 Å in **1a** (2.695 Å
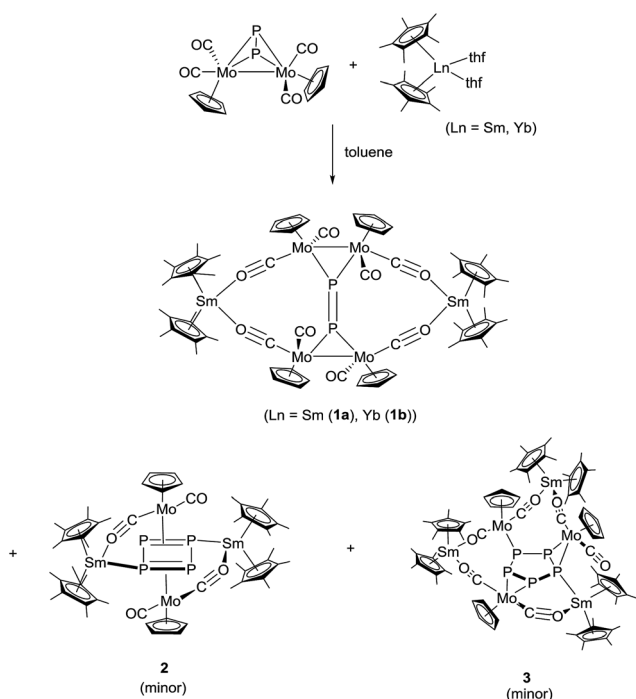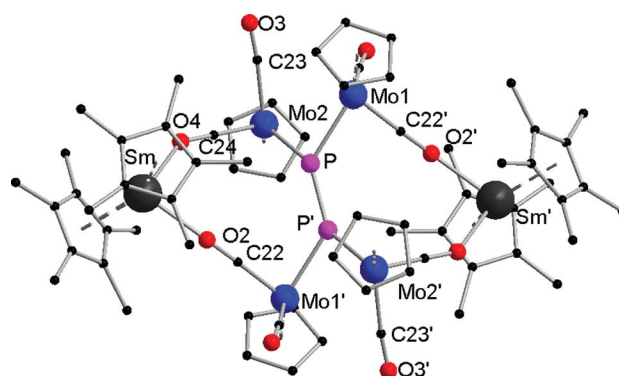

Scheme 2 Synthesis of **1–3**.

Fig. 1 Solid-state structure of **1a** (**1b** is similar). Hydrogen atoms are omitted for clarity. Selected distances [Å], angles [°]: **1a**: Sm–O2 2.359(5), Sm–O4 2.389(5), Mo1–Mo2 3.1935(8), Mo1–P 2.367(2), Mo1–C21 1.976(8), Mo1–C22' 1.881(8), Mo2–P 2.367(2), Mo2–C24 1.902(8), Mo2–C23 1.985(8), P–P' 2.029(4); O2–Sm–O4 83.4(2), C21–Mo1–P 110.7(2), C22–Mo1–P' 84.2(2), C21–Mo1–C22' 79.7(3), C23–Mo2–C24 83.9(3), C24–Mo2–P 87.7(2), P–Mo2–Mo1 47.57(5), P'–Mo1 132.88(13), P'–P–Mo2 132.71(12), Mo2–P–Mo1 84.86(6). **1b**: Yb–O2 2.231(5), Yb–O4 2.246(5), Mo1–Mo2 3.2073(9), Mo2–P 2.362(2), Mo1–C21 1.893(7), Mo1–C22 1.968(9), Mo2–P 2.362(2), Mo2–C23 1.974(8), Mo2–C24 1.863(7), P–P' 2.007(4); O2–Yb–O4 83.5(2), P–Mo1–Mo2 47.25(5), C21–Mo1–P 111.0(2), C21–Mo1–C22 82.6(3), C22–Mo1–P 86.0(2), P–Mo2–Mo1 47.13(4), C23–Mo2–P 108.9(3), C23–Mo2–C24 84.7(3), C24–Mo2–P 85.6(2), Mo1–P–Mo2 85.61(7).

(Sm1–C(Cp*1)(av.)) and 2.684 Å (Sm1–C(Cp*2)(av.))) in comparison to [Cp*$_2$Sm(thf)$_2$] (av. 2.86(3) Å)[14] and about 0.1 Å in **1b** (2.590 Å (Yb1–C(Cp*1)(av.)) and 2.583 Å (Yb1–C(Cp*2) (av.))) in comparison to [Cp*$_2$Yb(thf)] (av. 2.672 Å).[23] Similar Ln–C bond distances as in **1a,b** were observed in other trivalent complexes, *e.g.* in [Cp*$_2$SmCl(thf)] (av. 2.71 Å and 2.72 Å).[24]

In the IR spectra of **1a,b**, the CO stretching frequencies of the terminal CO ligands are observed as strong bands at 1945 cm^{-1}, 1905 cm^{-1} and 1871 cm^{-1} (**1a**), and 1906 cm^{-1} and 1873 cm^{-1} (**1b**) (Fig. S1 and S3†). Thus, they are in the range of [{CpMo(CO)$_2$}$_2$(μ,η$^{2:2}$-P$_2$)] (1965 cm^{-1}, 1913 cm^{-1}).[17] As expected, the bridging CO groups show stretching frequencies at lower energy (1683 cm^{-1}, 1636 cm^{-1} (**1a**) and 1687 cm^{-1}, 1638 cm^{-1} (**1b**)), which is also in agreement with the literature, *e.g.* 1650 cm^{-1} in [(Tp^{Me,Me})$_2$Sm(μ-CO){Cp^{Me}Mo(CO)$_2$}].[22]

As a result of weak ligand field splitting, Sm^{3+} complexes exhibit a characteristic absorption pattern in the NIR spectrum even in the presence of strong visible absorption.[25,26] The spectrum obtained for **1a** shows spectral patterns that are comparable to Sm^{3+}/POCl$_3$/ZrCl$_4$ (ref. 27) and Sm^{3+}/SeOCl$_2$/SnCl$_4$.[28] The observed bands at 9319 cm^{-1}, 8084 cm^{-1}, 7338 cm^{-1} and 6388 cm^{-1} for **1a** are assigned to the transitions of states $^6H_{5/2}$ → $^6F_{9/2}$, $^6F_{7/2}$, $^6F_{5/2}$, and $^6F_{1/2}$ respectively (Fig. S3†).[27]

The minor product **2** crystallizes in the triclinic space group $P\bar{1}$ with one molecule and one equivalent of toluene in the unit cell (Fig. 2). It consists of a central planar P$_4$ ring, which has a rectangular shape with two short (P1–P2 2.151(4) Å) and two long (P1–P2′ 2.265(3) Å) P–P bonds. Such a *cyclo*-tetraphosphabutadiene moiety was only recently reported in the Co(I) complex [(L^{Dep}Co)$_2$(μ$_2$:η^4,η^4-P$_4$)] (L^{Dep} = CH[C(Me)N(2,6-Et$_2$C$_6$H$_3$)]$_2$) as a result of P$_4$ activation.[29] In contrast, here for the first time, it is formed by merging two P$_2$ units together. A crystallographic inversion center is observed in the center of the P$_4$ ring. The angles within the P$_4$ ring (88.29(13)° and 91.71(13)°) are close to 90°. Two {CpMo(CO)$_2$} fragments each coordinate side-on in an

η^2-mode to the shorter P–P bonds, forming a [P$_4$(CpMo(CO)$_2$)$_2$]$^{2-}$ subunit. The angle between the P$_4$ ring and the Mo–P1–P2 plane is 108.77(13)°. As observed in **1a**, each {Cp*$_2$Sm}$^+$ unit coordinates *via* one isocarbonyl bridge to a {CpMo(CO)$_2$} fragment. The Sm atom is tilted towards the ring with an O1′–Sm–P1 angle of 76.8(2)°. The Sm–P1 distance of 3.016(3) Å is in agreement with other samarium phosphide compounds such as [Cp*FeP$_5$-Sm(DIP$_2$pyr)(THF)$_2$] (2.847(2) Å to 3.0703(15) Å)[11] and [(Cp*$_2$-Sm)$_4$P$_8$] (2.997(2) Å to 3.100(2) Å).[6] The observed isocarbonyl bridge in **2** (Sm–O1 2.388(7) Å) is in the range of **1a**.

Compound **3** crystallizes in the triclinic space group $P\bar{1}$ (Fig. 3). As a result of strong disorder, bonding parameters are not discussed in detail. The disorder is caused by two superimposed molecules (Fig. S4 and S5†), which could be separately refined. The central part of **3** consists of a planar P$_5$ ring. As observed in **2**, two {CpMo(CO)$_2$} fragments (Mo1, Mo2) coordinate side-on in an η^2-mode to the phosphorus ring. Mo1 binds to P1 and P2, and Mo2 binds to P3 and P4. A third {CpMo(CO)$_2$} fragment (Mo2′) binds to the remaining phosphorus atom (P5). The different coordination modes of Mo2 and Mo2′, and Sm1 and Sm1′, are a result of the disorder (see Fig. S4 and S5†). The two CO ligands of this unit each link Mo2′ to two {Cp*$_2$Sm}$^+$ units (Sm1′, Sm2) *via* isocarbonyl bridges. One additional isocarbonyl bridge from an adjacent {CpMo(CO)$_2$} fragment is also observed for both {Cp*$_2$Sm}$^+$ units. Thus, Sm1′ and Sm2 are each coordinated to two Cp* rings and two isocarbonyl ligands. The samarium atom of the third {Cp*$_2$Sm}$^+$ unit (Sm1) is coordinated to only one isocarbonyl ligand (from Mo1) and one phosphorus atom (P3) from the planar P$_5$ ring.

The formation of **1–3** is in contrast to other reported coordination derivatives of [{CpMo(CO)$_2$}$_2$(μ,η$^{2:2}$-P$_2$)]. In the known derivatives, such as [CuBr(Cp$_2$Mo$_2$(CO)$_4$P$_2$)]$_n$[30] and [{(CpMo(CO)$_2$P)$_2$}$_4$Ag$_2$][Al{OC(CF$_3$)$_3$}$_4$]$_2$,[31] the [CpMo(CO)$_2$P]$_2$ scaffold stayed intact. Even the addition of Lewis bases to the latter species did not cleave the Mo–P scaffold. Due to the reduction reported herein, the phosphorus atoms completely
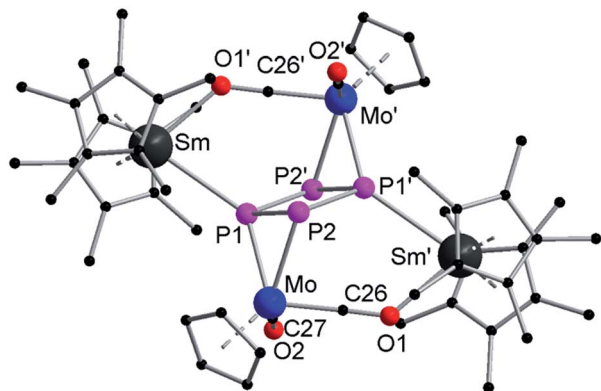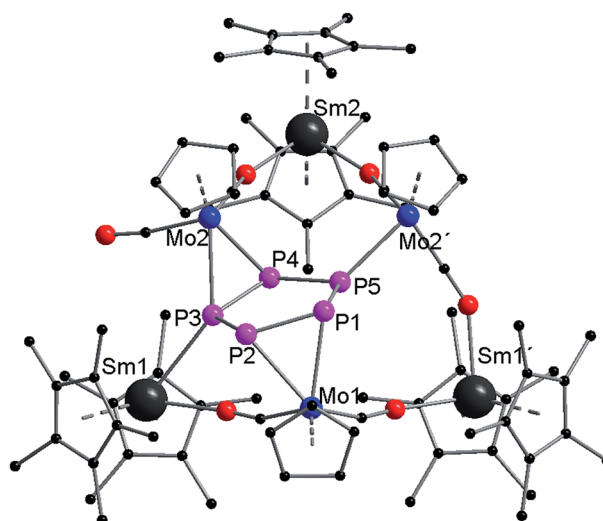

Fig. 2 Solid-state structure of **2**. Hydrogen atoms are omitted for clarity. Selected bond lengths [Å], angles [°]: Sm–P1 3.016(3), Sm–O1′ 2.388(7), Mo–P2 2.551(3), Mo–P1 2.525(3), Mo–C26 1.875(12), Mo–C27 1.968(11), P1–P2 2.151(4), P1–P2′ 2.265(3); O1′–Sm–P1 76.8(2), P1–Mo–P2 50.14(9), C26–Mo–C27 84.2(4), Mo–P1–Sm 137.26(10), P1–P2–Mo 64.31(10), P1–P2′–Mo′ 106.08(12), P1–P2–P1′ 88.29(13), P2–P1′–P2′ 91.71(13).

Fig. 3 Solid-state structure of **3**. Hydrogen atoms are omitted for clarity.

rearrange, forming P_2, P_4, and P_5 units. Obviously, strong reducing agents are needed to cleave the $[CpMo(CO)_2P]_2$ scaffold since the reducing power of $[Cp*_2Eu(thf)_2]$ is too weak to effect this reaction.

The nature of the bonding in **1a**, **2** and **3** was investigated by quantum chemical RI-DFT calculations using the program system TURBOMOLE.[32,33] The calculations were performed using the BP86 functional[34–36] by using the R-IJ approximation.[37] The basis sets for all atoms (except Sm) were of def-SV(P) quality.[38,39] For Mo and Sm, a relativistic corrected effective core potential was used to simulate the 28 (Mo)[40] and 51 inner electrons (ECP-51).[41] Due to the expected ionic nature of the complex containing Sm in the formal trivalent oxidation state, the inclusion of the 5f-electrons into the ECP is allowed. The structural results obtained for **1a** by crystallographic studies were confirmed by our theoretical calculations (**1a** (theory/exp.): d(P–P) 2.078/2.029, d(Mo–P) 2.406/2.367, d(Mo–Mo) 3.247/3.194 Å).

To gain insight into the nature of the bonding in **1a** and **2**, population analyses based on occupation numbers were performed (Roby–Davidson–Ahlrichs–Heinzmann population analysis).[42,43] The results were compared with those of the starting material $[\{CpMo(CO)_2\}_2(\mu,\eta^{2:2}\text{-}P_2)]$ and the model compound $(Na^+)_4(P_2)^{2-}$ possessing a P=P double bond. Partial charges (Q) to interpret the ionicity of the bonds were obtained. Shared electron numbers (SEN) served as a measure for the covalent bond strength. The analysis confirmed the realization of an ionic complex **1a** with regard to Sm (Q(Sm)) = +1.40); electron density was transferred from the π- and π*-type MOs of the P_2^{2-} unit to Mo (Q(P) = 0.00, Q(Mo) = −0.54; (see MOs 6 b_{2u}, 3 b_{1u} and 6 b_{1g} as well as 303 a, 312 a and 330 a in the MO diagrams given in the ESI†). This behavior leads to a reduced SEN as well as a larger distance of the P–P bond (SEN(P–P) = 1.38, r(P–P) = 207.8) compared to that of the typical P=P double bond in $(Na^+)_4(P_2)^{2-}$ (SEN(P–P) = 1.74, r(P–P) = 206.3). Comparison with the educt molecule $[\{CpMo(CO)_2\}_2(\mu,\eta^{2:2}\text{-}P_2)]$ (SEN(Mo–P) = 0.55, r(Mo–P) = 250.5) indicates a significant increase of the Mo–P bond strength in **1a**.

The observed P–P distances in **2** were also confirmed by theoretical methods. It indicates that the nature of the bonding in the central P_4 unit is comparable to that of a recently published Co(ɪ) complex.[29] Furthermore, some less significant similarities to the model compound D_{2h}–P_4 were seen (see ESI†). A similar situation is observed for the P–P bonds in **3**. The distances are in agreement with the anionic building block in well-known P_5^- complexes.[44,45] On the other hand the increase of the bond strength in the P_5 unit is compared to a P–P single bond less pronounced than in the calculated model compounds Na_2P_4, NaP_5, and $Na_3P_5^{2+}$ (distances and SEN given in the ESI†).

Due to the low symmetries and the sophisticated ligand sphere of metal complexes, complicated MO diagrams excluding a detailed bonding analysis were obtained for **2** and **3**. Thus, it cannot be excluded that the P_4 and P_5 units are mainly stabilized by the coordinating metal complex fragments and the observed P–P interactions are less significant.

To gain more insight into the reduction chemistry of molybdenum phosphides, we further treated $[Cp*_2Ln(thf)_2]$

(Ln = Sm, Yb) with $[Cp*Mo(CO)_2(\eta^3\text{-}P_3)]$,[46] which features a P_3 triangle in the coordination sphere. Reactions in toluene at 60 °C resulted in 4d/4f hexaphosphides $[(Cp*_2Ln)_2P_6\text{-}(Cp*Mo(CO)_2)_2]$ (Ln = Sm (**4**), Yb (**5**)) (Scheme 3). The solid-state structures of both compounds were established by single crystal X-ray diffraction (Fig. 4). Compounds **4** and **5** are isostructural and crystallize in the triclinic space group $P\bar{1}$. The solid-state structures of **4** and **5** are disordered. The central P_6 core shows four-fold disorder (Fig. S6 and S7†). Thus, bonding parameters are not discussed in detail. Fig. 4 shows only one of the disordered positions. The formation of **4** and **5** is easier to rationalize than the formation of **1–3**. Due to the one-electron reduction of $[Cp*Mo(CO)_2(\eta^3\text{-}P_3)]$, one Mo–P bond is broken and a new P–P bond (P2–P2' in **4**) between two negatively charged 18 VE $[Cp*Mo(CO)_2P_3]^-$ units is formed. The P–P bond length of the newly formed bond is in the range of a P–P single bond (2.154(3) Å (**4**) and 2.216(6) Å (**5**)).[47] A crystallographic inversion center is observed in the middle of this central P–P bond. The negative charge of the $[Cp*Mo(CO)_2P_3]^-$ units is a result of the one-electron reduction by the lanthanocenes. For charge balance, two $\{Cp*_2Sm\}^+$ units coordinate to the central $\{P_6\text{-}(Cp*Mo(CO)_2)_2\}^{2-}$ scaffold. The $\{Cp*Mo(CO)_2\}$ units in **4** and **5** bind side-on in an η^2-mode to the central P_6 core. As observed in **2**, each $\{Cp*_2Ln\}^+$ cation coordinates to the molybdenum atom *via* one isocarbonyl bridge. The Ln–O distances (av. (including all disordered positions) 2.409 Å (**4**) and 2.311 Å (**5**)) are in the range of other isocarbonyl compounds, *e.g.* $[(Tp^{Me,Me})_2Sm\text{-}(\mu\text{-}CO)(CpMo(CO)_2)]$ (2.335(4) Å), $[(Cp*_2Sm)(\mu\text{-}CO)_2(Cp*Fe)]_2$ (2.348(4) Å), $[(Cp*_2Yb)(\mu\text{-}CO)_2Mn(CO)_3]_2$ (2.271(2) Å) and $[(Cp*_2Yb(thf))(\mu\text{-}CO)Co(CO)_3]$ (2.258(2) Å).[16,48] Furthermore, coordination of the lanthanide atoms to the P_6 core is observed and Ln–P1 bonds of 2.963(2) Å (**4**) and 2.879(3) Å (**5**) are formed. The observed Yb–P distances correspond well with those of comparable compounds with Yb–PR_3 interactions, *e.g.* $[Li(thf)_4]$ $[(Ph_2PNPh)_4Yb]$ (2.885(2)–3.031(2) Å).[49] As already observed in **2**, the lanthanide atoms are coordinated to two Cp* rings, one phosphorus, and one oxygen atom from the isocarbonyl bridge.

The IR spectra show intense bands for the CO stretching vibrations at 1917 cm^{-1} (**4**) and 1916 cm^{-1} (**5**), respectively, which can be assigned to the terminal non-bridging CO ligands. Absorption bands at 1701 cm^{-1} (**4**), and 1696 and 1669 cm^{-1} (**5**), are assigned to the isocarbonyl ligands (Fig. S9 and S11†). This assignment is in agreement with related compounds, *e.g.* $[(Cp*_2\text{-}Yb)(\mu\text{-}CO)_2Mn(CO)_3]_2$ and $[(Tp^{Me,Me})_2Sm(\mu\text{-}CO)(CpCr(CO)_2)]$.[16,22]
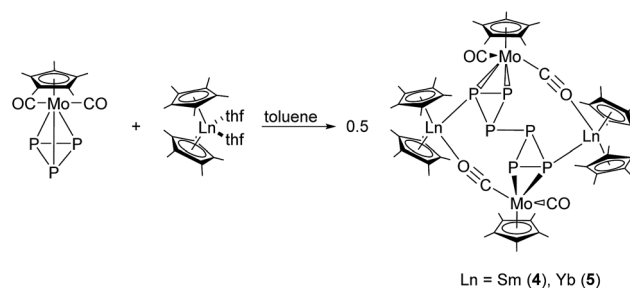
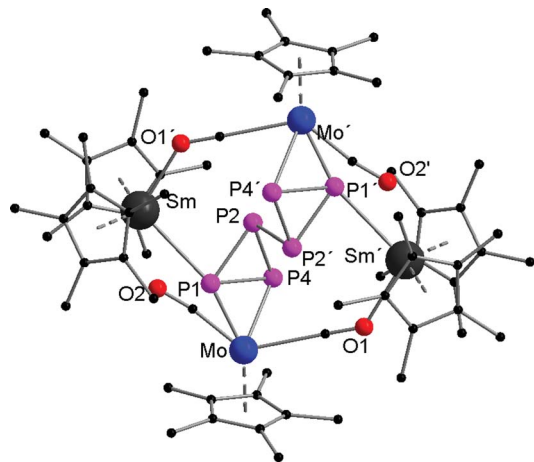**Scheme 3** Synthesis of **4** and **5**.

Fig. 4 Solid-state structure of **4** (**5** is isostructural). Hydrogen atoms are omitted for clarity.

To support the formation pathway of **4** and **5**, the oxidation state of the samarium atom in **4** was determined by magnetic measurements (SQUID) and NIR spectroscopy. Low paramagnetic susceptibility χ_M (290 K) = 6238 × 10^{-6} cm^3 mol^{-1} and magnetic moment μ_{eff} = 3.80 μ_B correspond to the two samarium(III) metal centers and two unpaired electrons from the Mo atoms in **4** (Fig. S9†). These data are comparable to the literature values for Sm^{3+} complexes.[11]

As described for **1**, the oxidation state of the samarium atom in **4** was unambiguously assigned by NIR spectroscopy.[25,26] The observed bands at 9224 cm^{-1}, 7967 cm^{-1}, 6702 cm^{-1} and 6395 cm^{-1} are assigned to the transitions of states $^6H_{5/2} \rightarrow {}^6F_{9/2}$, $^6F_{7/2}$, $^6F_{3/2}$ and $^6F_{1/2}$ (Fig. S11†).[27]

Conclusions

In summary, we have synthesized and characterized the first 4d/4f polyphosphides. Reduction of molybdenum polyphosphides with the divalent lanthanocences [Cp*$_2$Ln(thf)$_2$] (Ln = Sm, Yb) resulted in the reduction of the molybdenum compounds in both cases. Depending on the nature of the molybdenum polyphoshide, different reaction pathways were followed. Reduction of the mononuclear complex [Cp*Mo(CO)$_2$(η^3-P$_3$)] leads to a breaking of one Mo–P bond and the formation of a new P–P bond of a central P$_6$ core in the {P$_6$(Cp*Mo(CO)$_2$)$_2$}$^{2-}$ fragment.

In contrast, the reduction pathway of [{CpMo(CO)$_2$}$_2$($\mu,\eta^{2:2}$-P$_2$)] is more diverse. This reduction always results in a rearrangement of the P$_2$ unit. In the major product, a {P=P}$^{2-}$ unit is observed, which is the result of a two electron reduction. In some cases also aggregation of the phosphorus scaffolds occurs, forming novel planar *cyclo*-tetraphosphabutadiene P$_4$ and *cyclo*-P$_5$ fragments by P–P bond formations in an unprecedented coordination environment. These polyphosphides are surrounded by {CpMo(CO)$_2$} fragments.

In each compound, the lanthanocene cations {Cp*$_2$Ln}$^+$ are bound *via* isocarbonyl bridges, and in some cases also *via* Ln–P bonds, to the molybdenum polyphosphide core.

The present and earlier results contribute to our preliminary understanding of reduction reactions of transition metal polyphosphides by divalent lanthanide species. In each case a reduction and the rearrangement of the phosphorus scaffold takes place. This results predominantly in the aggregation of the polyphosphide units by the formation of novel P–P bonds.

Notes and references

1 J. H. Downing and M. B. Smith, in *Comprehensive Coordination Chemistry II*, ed. J. A. M. J. Meyer, Pergamon, Oxford, 2003, pp. 253–296.
2 K. B. Dillon, F. Mathey and J. F. Nixon, *Phosphorus: The Carbon Copy*, Wiley, Chichester, U.K., 1998.
3 H. Butenschön, *Chem. Rev.*, 2000, **100**, 1527–1564.
4 M. Peruzzini and L. Gonsalvi, *Phosphorus Compounds-Advanced Tools in Catalysis and Material Sciences*, Springer, Netherlands, 2011.
5 T. Li, S. Kaercher and P. W. Roesky, *Chem. Soc. Rev.*, 2014, **43**, 42–57.
6 S. N. Konchenko, N. A. Pushkarevsky, M. T. Gamer, R. Köppe, H. Schnöckel and P. W. Roesky, *J. Am. Chem. Soc.*, 2009, **131**, 5740–5741.
7 W. Huang and P. L. Diaconescu, *Chem. Commun.*, 2012, **48**, 2216–2218.
8 W. Huang and P. L. Diaconescu, *Eur. J. Inorg. Chem.*, 2013, **2013**, 4090–4096.
9 Y. Lv, X. Xu, Y. Chen, X. Leng and M. V. Borzov, *Angew. Chem., Int. Ed.*, 2011, **50**, 11227–11229.
10 T. Li, M. T. Gamer, M. Scheer, S. N. Konchenko and P. W. Roesky, *Chem. Commun.*, 2013, **49**, 2183–2185.
11 T. Li, J. Wiecko, N. A. Pushkarevsky, M. T. Gamer, R. Köppe, S. N. Konchenko, M. Scheer and P. W. Roesky, *Angew. Chem., Int. Ed.*, 2011, **50**, 9491–9495.
12 M. V. Butovskiy, G. Balázs, M. Bodensteiner, E. V. Peresypkina, A. V. Virovets, J. Sutter and M. Scheer, *Angew. Chem., Int. Ed.*, 2013, **52**, 2972–2976.
13 T. Li, N. Arleth, M. T. Gamer, R. Köppe, T. Augenstein, F. Dielmann, M. Scheer, S. N. Konchenko and P. W. Roesky, *Inorg. Chem.*, 2013, **52**, 14231–14236.
14 W. J. Evans, I. Bloom, W. E. Hunter and J. L. Atwood, *J. Am. Chem. Soc.*, 1981, **103**, 6507–6508.
15 W. J. Evans, T. A. Ulibarri, H. Schumann and S. Nickel, in *Inorg. Synth.*, John Wiley & Sons, 2007, pp. 155–157.
16 J. M. Boncella and R. A. Andersen, *Inorg. Chem.*, 1984, **23**, 432–437.

17 O. J. Scherer, H. Sitzmann and G. Wolmershäuser, *J. Organomet. Chem.*, 1984, **268**, C9–C12.

18 C. E. Kefalidis, S. Essafi, L. Perrin and L. Maron, *Inorg. Chem.*, 2014, **53**, 3427–3433.

19 O. J. Scherer, M. Ehses and G. Wolmershäuser, *Angew. Chem., Int. Ed.*, 1998, **37**, 507–510.

20 G. Lin and W.-T. Wong, *J. Organomet. Chem.*, 1996, **522**, 271–275.

21 G. Parkin, *Struct. Bonding*, 2010, **136**, 123.

22 A. C. Hillier, S. Y. Liu, A. Sella, O. Zekria and M. R. J. Elsegood, *J. Organomet. Chem.*, 1997, **528**, 209–215.

23 T. D. Tilley, R. A. Andersen, B. Spencer, H. Ruben, A. Zalkin and D. H. Templeton, *Inorg. Chem.*, 1980, **19**, 2999–3003.

24 S. N. Konchenko, T. Sanden, N. A. Pushkarevsky, R. Köppe and P. W. Roesky, *Chem.–Eur. J.*, 2010, **16**, 14278–14280.

25 C. M. Lukehart, *Fundamental Transition Metal Organometallic Chemistry*, Brooks Cole, Belmont, 1988.

26 W. J. Evans, J. W. Grate, K. R. Levan, I. Bloom, T. T. Peterson, R. J. Doedens, H. Zhang and J. L. Atwood, *Inorg. Chem.*, 1986, **25**, 3614–3619.

27 A. C. Hillier, A. Sella and M. R. J. Elsegood, *J. Chem. Soc., Dalton Trans.*, 1998, 3871–3874.

28 A. Recknagel, A. Steiner, S. Brooker, D. Stalke and F. T. Edelmann, *Chem. Ber.*, 1991, **124**, 1373–1375.

29 S. Yao, N. Lindenmaier, Y. Xiong, S. Inoue, T. Szilvási, M. Adelhardt, J. Sutter, K. Meyer and M. Driess, *Angew. Chem., Int. Ed.*, 2015, **54**, 1250–1254.

30 J. Bai, E. Leiner and M. Scheer, *Angew. Chem., Int. Ed.*, 2002, **41**, 783–786.

31 M. Scheer, L. J. Gregoriades, M. Zabel, J. Bai, I. Krossing, G. Brunklaus and H. Eckert, *Chem.–Eur. J.*, 2008, **14**, 282–295.

32 O. Treutler and R. Ahlrichs, *J. Chem. Phys.*, 1995, **102**, 346–354.

33 R. Ahlrichs, M. Bär, M. Häser, H. Horn and C. Kölmel, *Chem. Phys. Lett.*, 1989, **162**, 165–169.

34 A. D. Becke, *Phys. Rev. A*, 1988, **38**, 3098–3100.

35 J. P. Perdew, *Phys. Rev. B: Condens. Matter Mater. Phys.*, 1986, **33**, 8822–8824.

36 J. P. Perdew, *Phys. Rev. B: Condens. Matter Mater. Phys.*, 1986, **34**, 7406.

37 M. Sierka, A. Hogekamp and R. Ahlrichs, *J. Chem. Phys.*, 2003, **118**, 9136–9148.

38 F. Weigend, *Phys. Chem. Chem. Phys.*, 2006, **8**, 1057–1065.

39 F. Weigend and R. Ahlrichs, *Phys. Chem. Chem. Phys.*, 2005, **7**, 3297–3305.

40 D. Andrae, U. Häußermann, M. Dolg, H. Stoll and H. Preuß, *Theor. Chim. Acta*, 1990, **77**, 123–141.

41 M. Dolg, H. Stoll, A. Savin and H. Preuss, *Theor. Chim. Acta*, 1989, **75**, 173–194.

42 R. Ahlrichs and C. Ehrhardt, *Chem. Unserer Zeit*, 1985, **19**, 120–124.

43 R. Heinzmann and R. Ahlrichs, *Theor. Chim. Acta*, 1976, **42**, 33–45.

44 O. J. Scherer and T. Brück, *Angew. Chem., Int. Ed.*, 1987, **26**, 59.

45 M. Detzel, T. Mohr, O. J. Scherer and G. Wolmershäuser, *Angew. Chem., Int. Ed.*, 1994, **33**, 1110–1112.

46 O. J. Scherer, H. Sitzmann and G. Wolmershäuser, *Angew. Chem.*, 1985, **97**, 358–359.

47 M. Häser and O. Treutler, *J. Chem. Phys.*, 1995, **102**, 3703–3711.

48 T. D. Tilley and R. A. Andersen, *J. Chem. Soc., Chem. Commun.*, 1981, 985–986.

49 T. G. Wetzel, S. Dehnen and P. W. Roesky, *Angew. Chem., Int. Ed.*, 1999, **38**, 1086–1088.